

Supplemental Material: Details of the experiments, analysis, and modeling

Hydrothermal experiments

Starting material: Sample solutions were prepared at room temperature from reagent grade chemicals (ZnCl₂, PbCl₂, BaCl₂, and NaCl), and acidified using HCl to around pH = 2-3 at 25°C. Non-acidified solutions were also used as initial fluids for comparison. The solution salinity of 1.7 to 3 m (9~15 wt% NaCl) is within the range of the ore fluid salinity (4-28wt% NaCl) for the sediment-hosted Zn-Pb deposits (Wilkinson, 2014), and the chosen Zn content is based on the estimation of Zn and Pb concentration near the upper limit of the measured values from fluid inclusions in sphalerite (Wilkinson et al., 2009) with the arbitrary concentration of other components added. Calcite and dolomite crystals were crushed to 200 µm to 1 mm size, then rinsed with distilled water and dried before use. The solution compositions are listed in Table S1.

Table S1 Details of sample compositions, solution pH and main reaction products for hydrothermal experiment (anh: Anhydrite; ga: galena; sp: sphalerite; bar: barite)

Sample Numbers	Initial solids	Initial fluid composition	initial pH @25C	Final pH @25C	main S-bearing minerals
R5-3, 5-4,	S, calcite	0.07 m ZnCl ₂ , 3.0 m NaCl	2, 2.3	6.1	sp, anh
R3	S, dolomite	0.07 m ZnCl ₂ , 3.0 m NaCl	2.0	7.5	sp, anh
R9-6	S, calcite	0.07 m ZnCl ₂ , 0.01 m PbCl ₂ , 3.0 m NaCl	2.4	6.0	sp, ga, anh
R11-1	S, calcite	0.1 m ZnCl ₂ , 1.7 m NaCl, 0.2 m MgCl ₂ ,	5.9	6.3	sp, anh
R16-1	S, calcite	0.07 m ZnCl ₂ , 3.0 m NaCl, 0.1 m BaCl ₂	2.3	6.5	Sp, bar
R16-1S	S only	0.07 m ZnCl ₂ , 3.0 m NaCl, 0.1 m BaCl ₂	2.3	1.0	no precipitates
R12-5, R17-1	S, calcite	0.1 m ZnCl ₂ , 1.7 m NaCl, 0.1 m BaCl ₂ , 0.2 m MgCl ₂ , 0.15 m CaCl ₂ , 0.01 m PbCl ₂	2.9, 2.4	6.5	sp, ga, bar,
R12-5S	S only	0.1 m ZnCl ₂ , 1.7 m NaCl, 0.2 m MgCl ₂ , 0.15 m CaCl ₂ , 0.01 m PbCl ₂	2.4	0.6	S
R17-3	S, dolomite	0.1 m ZnCl ₂ , 1.7 m NaCl, 0.2 m MgCl ₂ , 0.15 m CaCl ₂ , 0.01 m PbCl ₂	2.4	6.0	sp, ga, bar,

Experiments were conducted in Teflon-lined stainless autoclaves, with ~30 ml of internal volume. For each run, ~0.1 g of elemental sulfur and ~0.4 g of calcite or dolomite are loaded into the autoclave, then added are ~10 ml of the prepared solution. Native sulfur is

used as the source of reduced sulfur, as native sulfur produces both reduced sulfur and sulfate upon heating above 120 °C (Ellis and Giggenbach, 1971), and the reaction also buffers the redox state near sulfide/sulfate boundary:



Where 4 moles of native sulfur disproportionate to three moles of H₂S and one mole of SO₄²⁻, and thermodynamic calculations show that pH values of typical experimental solutions (3 molal NaCl, 0.35 m S) are around 2.2. The loaded autoclaves were placed in a fan-circulated oven with Eurotherm temperature controller with a temperature precision of ±1 °C. Experiments are conducted at 200°C and solution-saturated pressure. The 200°C temperature is within the range of ore-forming temperature range of 100-250°C (SEDEX: 100-150°C, MVT and Irish Type, 84-250°C; Wilkinson, 2014), and also helps reactions proceed faster than lower temperatures. After two days at 200 °C, all the elemental sulfur had been converted to sulfate and sulfide. All experimental runs lasted 2-3 weeks to ensure completion of reactions.

After the experiments, the autoclaves are taken out of the oven and cooled with a fan for ~30 min to room temperature. The solution was then retrieved for pH measurement and concentration analysis of selected elements (Table S3) using Inductively coupled plasma atomic emission spectroscopy (ICP-OES). The solid products were washed and dried under ambient condition before Scanning Electron Microscopy (SEM), Electron Probe Microanalysis (EPMA) and Electron Backscatter Diffraction (EBSD) work.

SEM Examination and Sample preparation

Solid samples were examined in SEM in both "as produced" form and cross-section. For the "as produced" samples, crystallites from the experiment were dried and mounted directly on standard SEM double-sided, conductive carbon tape and examined in the SEM in low vacuum mode at a pressure of 0.5 torr, uncoated. A beam energy of 15 keV and a probe current of approximately 0.8 nA were used and both secondary electron (SE) and backscattered electron (BSE) images were collected.

For the polished cross-sections, samples were mounted using Struers Epofix epoxy resin in a 25 mm round block, then mechanically prepared, first using SiC papers in the sequence 320, 600 and 1200 grit with non-aqueous lubrication and second using diamond laps in the sequence 6, 3, 1 and 0.25 µm, again, using non-aqueous lubrication. After mechanical polishing, the sample had a 4 nm carbon coat applied using a Leica ACE600 thin

film coater, then EPMA analysis was carried out. Following EPMA analysis and in preparation for EBSD analysis, the sample was argon ion beam milled in the sequence 10 keV for 5 mins at a milling angle of 3°, 2 keV for 10 mins, 1 keV for 10 mins and 0.4 keV for 5 mins, all with a milling angle of 5° and constant stage rotation. A Technoorg Linda model SEM Prep2 was used for this stage of the sample preparation to minimize any amorphous layers introduced by the mechanical polishing (Suess et al., 2011, Glenn et al. 2020). Again, the sample was coated with a 4 nm layer of carbon prior to EBSD analysis. Both the ion beam polisher and carbon coater had base vacuums in the 10⁻⁵ Pascal range.

EPMA mapping

A JEOL JXA 8500F-CL electron probe microanalyzer was used to collect the maps and quantitative point analyses. The EPMA mapping conditions were 12 keV, 25 nA, 40 ms dwell, the pixel step size and beam defocus were both set to 200 nm, Fig. 1(g) and Fig. 1(i). These conditions were chosen to be a compromise between good CL and x-ray production that were of adequate signal-to-noise at a pixel for fitting to be utilized. Wavelength dispersive spectrometers, energy dispersive spectrometers and spectral cathodoluminescence signals were all collected in parallel (MacRae et al. 2013). Mapping data were analyzed using Chimage X in-house software (Harrowfield et al. 1993, Torpy et al. 2020).

Microanalysis conditions

Quantitative EPMA was performed at an accelerating voltage of 15 kV and a beam current 15 nA. The electron beam was defocused to 2 mm for the analyses. The suite of elements analyzed included Mg, S, Ca, Zn, Ba, Pb and O. Standards used were barite (BaSO₄), sphalerite (ZnS), wollastonite (CaSiO₃), galena (PbS) and spinel (MgAl₂O₄). Standards and the unknown were coated at the same time to minimize absorption problems associated with different carbon coat thicknesses. Oxygen was measured directly using the peak and background high and low procedure. Peak counting times were 20 seconds for all elements except Ca, S and Ba which were set to 10 seconds. Under these conditions, the detection limits (2σ) were generally less than 300 ppm for all elements. The quantification was applied using the library of Stratagem®, a software based on the work of Pouchou and Pichoir (1992). The results of quantitative EPMA analysis are shown in Table S2.

Table S2 Quantitative EPMA spot analysis of the weight percentage of the selected elements for the spots marked on Fig. 3. (ga: galena; sp: sphalerite; brc: brucite; bar: barite)

Point	O	Zn	S	Ba	Ca	Pb	Mg	Total	Mineral
1	5.69	60.47	28.17	0.05	0.00	0.86	0.09	95.33	sp
2	6.20	63.79	29.91	0.00	0.00	1.18	0.06	101.14	sp
3	5.82	63.45	29.92	0.08	0.01	0.98	0.03	100.28	sp
4	5.42	64.46	31.02	0.01	0.00	0.79	0.02	101.71	sp
5	5.35	64.68	30.97	0.02	0.01	1.22	0.01	102.26	sp
6	21.71	-0.11	11.64	62.15	0.06	0.00	0.01	95.47	bar
7	22.15	0.03	11.99	60.94	0.06	0.00	0.00	95.17	bar
17	49.90	0.05	0.28	0.02	0.02	0.00	45.72	95.99	brc
18	50.16	0.09	0.14	0.05	0.02	0.00	45.38	95.84	brc

EBSD

EBSD analysis was performed in a FEI Quanta 400, field emission, environmental scanning electron microscope (ESEM) equipped with a Bruker eFlash EBSD detector and Bruker Esprit ver 2.2 acquisition software. An area measuring $140.5 \times 121.3 \mu\text{m}$ was mapped using a resolution of 1024×884 pixels. A dwell time of 150 ms was used, generating a total collection time of approximately 75 hrs. 5×5 binning was used, creating diffraction patterns of 320×240 pixels and a Hough resolution of 99 pixels. Phase cards for sphalerite, wurtzite, galena and barite were taken from the international crystal structure database (ICSD) or the American Mineralogist crystal structure database (AMSCD). Band detection for acquisition was set to a maximum of 12 bands and a minimum of 7 or 8 bands and a maximum mismatch angle of 1.5° was used for the display of results. Post processing of the results was also done using Bruker Esprit 2.2 software using a minimum of 5° misorientation to define a grain and a minimum grain size of 5 pixels. No "cleaning" procedures whatsoever have been applied to any of the EBSD data displayed in this research.

Thermodynamic modelling

Thermodynamic modelling for the experimental systems and ore fluid mixing was conducted using Geochemist's Workbench modelling package (Bethke, 2007), with the b-dot extension of Debye-Huckle activity model (Helgeson et al., 1969). The thermodynamic properties for Zn chloride complexes are from Mei et al. (2015), and Zn hydrosulfide complexes are from Tagirov and Seward (2010). The properties for Pb chloride complexes are from Etschmann et al. (2018), and the rest of the thermodynamic data are from the default

LLNL thermodynamic database (version thermo.com.R7beta) (Wolery, 1992). Equilibrium constants for the reactions of sphalerite and galena deposition from ZnCl_4^{2-} and PbCl_3^- reacting with $\text{H}_2\text{S}(\text{aq})$, respectively, are listed in Table S3.

Table S3 Equilibrium constants for the reactions of ZnCl_4^{2-} and PbCl_3^- with $\text{H}_2\text{S}(\text{aq})$ to precipitate sphalerite and galena, respectively.

T (°C)	0	25	60	100	150	200	250	300
$\text{ZnCl}_4^{2-} + \text{H}_2\text{S}(\text{aq}) = \text{ZnS}_{(\text{sphalerite})} + 4\text{Cl}^- + 2\text{H}^+$	5.32	5.16	3.77	2.2	0.31	-1.56	-3.52	-5.81
$\text{PbCl}_3^- + \text{H}_2\text{S}(\text{aq}) = \text{PbS}_{(\text{galena})} + 3\text{Cl}^- + 2\text{H}^+$	6.98	6.01	4.72	3.29	1.52	-0.32	-2.39	-4.95

Speciation calculations have been conducted to predict mineral phases and final solution compositions for the selected experimental systems and compared to the observed major mineral phases and ICP-OES analysis of the elemental concentrations of the resultant solutions (Table S4). An example of predicted mineral phases is shown in Fig S1. The predicted sulfide minerals are sphalerite, barite and galena, and minor dolomite (Fig. S1a), consistent with the observed mineral assemblages, except that brucite instead of dolomite is observed, probably due to the more reduced condition than prediction in the experiment, favoring the formation of brucite over dolomite (Etschmann et al., 2014). For the same reaction without calcite (R12-5S), no precipitation of sphalerite was predicted, and initially-precipitated galena redissolved with decreasing pH as the reaction proceeded (Fig. S1b), which is consistent with the experimental observations of no sphalerite and galena in the reaction product. However, precipitation of barite is predicted but not observed, also probably due to the reducing conditions in the experiment, causing a lack of sulfate to form barite, with Ba stays in the resultant solution (Table S4). The calculated concentrations of Pb and Zn of the resultant solutions are consistent with the ICP-OES measurement (Table S4).

Table S4 Element concentrations (g/L) of the solution phase of experimental product for representative samples calculated with thermodynamic modelling (Calc.), and ICP-OES analysis (Meas.) The typical uncertainties of ICP-OES results are 2%, but Na and Cl concentrations are semi-quantitative due to large dilution factors.

	R5-4		R3		R16-1		R16-1S		R12-5		R12-5S	
	Calc.	Meas.	Calc.	Meas.	Calc.	Meas.	Calc.	Meas.	Calc.	Meas.	Calc.	Meas.
Ba	-	-	-	-	0.14	1.7	8.15	11	0.1	1.7	7.2	12
Ca	2.8	4.9	1.4	1.4	5.6	10	-	-	11.6	19	5.0	6.5
Cl	91.4	123	91	120	88	160	87.8	160	63	136	63	110
Mg	-	-	0.9	2		-	-	-	4.1	6.3	4.1	5.6
Na	56.3	74	59.2	75.2	50.1	91	50.8	90	19.8	55	19.8	45
Pb	-	-	-	-		-	-	-	0.0004	<0.005	1.7	2.3
S	3.2	2.9	2.76	3.4	4.8	2.8	1.4	<0.1	3.9	3.5	1.6	0.1
Zn	2.7e-05	<0.01	1.0e-04	<1	3.8e-05	<0.05	3.8	6.3	0.0002	<0.01	5.6	7.5

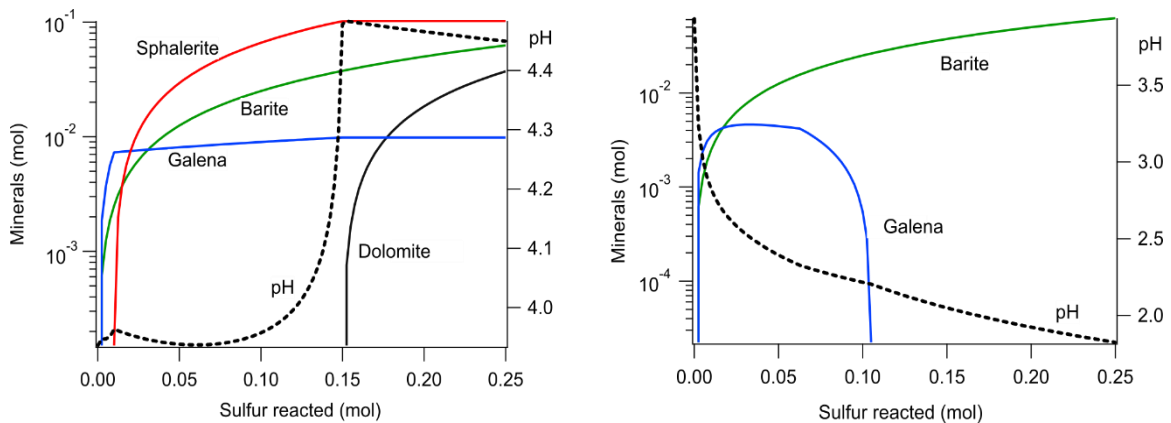


Fig. S1 Prediction of mineral products based on thermodynamic modelling for the experiment of a Zn-Pb-Ba-bearing NaCl brine reacting with native sulfur and calcite at 200 °C (Experiment R12-5) (a), and reacting with native sulfur only (b). See Table S1 for sample compositions.

In the thermodynamic modeling of fluid mixing of Zn-bearing brine with $H_2S_{(aq)}$, arbitrary Zn (1000 ppm), Pb (200 ppm) and Ba (500 ppm) concentrations are chosen. Those values fall within the ranges of metal concentrations reported for sediment-hosted Zn-Pb deposits. For example, 100-1000 ppm for Zn and Ba transport window for Zn-Pb-Ag deposits in Northern Australia (Large et al., 2005), to 3000 ppm Zn and several hundred ppm Pb for

Tri-State and Northern Arkansas, and 5000 ppm Zn and 5980 ppm Ba for Irish sphalerite (Stoffell et al., 2008; Wilkinson et al. 2009; Wilkinson and Hitzman, 2015).

The salinity of the starting fluids was set to 3 molal NaCl (~14.9 wt%), the upper limit of the B-dot activity coefficient model used (Bethke, 2007), also in the range of salinity (4-28 wt%) for major types of sediment-hosted Zn-Pb deposits (see reviews of Leach et al., 2005; Large et al., 2005; Wilkinson, 2014). The modeling results are shown in Table S5. Using calcite instead of dolomite yielded similar results.

Table S5 Calculated final pH, log fO_2 , and Ba, Pb and Zn concentrations as a result of mixing metal bearing brines with $H_2S(aq)$ with and without carbonate (dolomite) at 150 and 250°C. The starting metal concentrations are: Zn = 1000 ppm, Pb = 200 ppm and Ba = 500 ppm. The predominant Zn, Pb and Ba aqueous species are $ZnCl_4^{2-}$, $PbCl_3^-$, and $BaCl^+$, and the precipitated Zn, Pb and Ba mineral phases are sphalerite, galena and barite, respectively.

	T (°C)	Reaction path in Fig. 4	Starting pH	Final pH	Starting log fO_2	Final log fO_2	Final Ba (ppm)	Final Pb (ppm)	Final Zn (ppm)
With dolomite	150	A-D	2.0	5.3	-35.0	-47.7	29.5	0.2	0.02
		B-D	5.5	5.2	-35.0	-47.6	33.6	0.2	0.01
		C-D	2.0	5.2	-47.0	-47.7	33.6	0.2	0.01
	250	A-D	2.0	5.5	-28.0	-36.9	365.4	0.8	0.4
		B-D	5.5	5.6	-28.0	-37.0	282.9	0.9	0.5
		C-D	2.0	5.5	-35.0	-37.0	365.4	0.8	0.4
No dolomite	150	A-C	2.0	1.8	-35.0	-46.0	497.3	30.5	878.2
		B-C	5.5	1.9	-35.0	-46.0	497.5	22.4	649.2
	250	A-C	2.0	2.0	-28.0	-34.3	497.1	198.8	994.2
		B-C	5.5	3.1	-28.0	-35.0	497.2	77.3	994.4

References cited in Supplemental Materials

- Bethke, C.M., 2007, *Geochemical and Biogeochemical Reaction Modeling*, Second edition. Cambridge University Press, Cambridge.
- Ellis, A.J. and Giggenbach, W., 1971, Hydrogen sulphide ionization and sulphur hydrolysis in high temperature solution. *Geochimica et Cosmochimica Acta* 35, 247-260.
- Etschmann, B., Brugger, J., Pearce, M.A., Ta, C., Brautigan, D., Jung, M. and Pring, A., 2014, Grain boundaries as microreactors during reactive fluid flow: experimental dolomitization of a calcite marble. *Contributions to Mineralogy and Petrology* 168, 1045.

- Etschmann, B.E., Mei, Y., Liu, W., Sherman, D., Testemale, D., Müller, H., Rae, N., Kappen, P. and Brugger, J., 2018, The role of Pb(II) complexes in hydrothermal mass transfer: An X-ray absorption spectroscopic study. *Chemical Geology* 502, 88-106.
- Glenn, M., S. Hu, S. Barnes, A. Torpy, A. E. Hughes, C. M. MacRae, N. A. S. Webster, N. C. Wilson, J. Parr and R. Binns, 2020, Investigation of the Internal Structure of a Modern Seafloor Hydrothermal Chimney with a Combination of EBSD, EPMA, and XRD. *Microscopy and Microanalysis*: 1-15.
- Harrowfield I.R., MacRae C.M., and Wilson N.C., 1993, Chemical imaging in electron microprobes. *Microbeam Analysis* 2, 547–548.
- Helgeson, H.C., 1969, Thermodynamics of hydrothermal systems at elevated temperatures and pressures. *American Journal of Science* 267, 729-804.
- Large, R.R., Bull, S.W., McGoldrick, P.J., Walters, S., Derrick, G.M., Carr, G.R., Hedenquist, J.W., Thompson, J.F.H., Goldfarb, R.J. and Richards, J.P., 2005, Stratiform and Strata-Bound Zn-Pb-Ag Deposits in Proterozoic Sedimentary Basins, Northern Australia, One Hundredth Anniversary Volume. *Society of Economic Geologists*, p. 931-963.
- MacRae, C. M., Wilson, N. C. and Torpy, A., 2013, Hyperspectral cathodoluminescence. *Mineralogy and Petrology* 107, 429 - 440.
- Mei, Y., Sherman, D.M., Liu, W., Etschmann, B., Testemale, D. and Brugger, J., 2015, Zinc complexation in chloride-rich hydrothermal fluids (25-600 °C): A thermodynamic model derived from ab initio molecular dynamics. *Geochimica Et Cosmochimica Acta* 150, 265-284.
- Pouchou J. L. and Pichoir F., 1992, Quantitative analysis of homogeneous or stratified microvolumes applying the model PAP. in K.F.J. Heinrich, D.E. Newbury (Eds.), *Electron Probe Quantitation*, Plenum Press, New York, pp. 31-75
- Shvarov, Y.V., 2008, HCh: New potentialities for the thermodynamic simulation of geochemical systems offered by windows. *Geochemistry International* 46, 834-839.
- Stoffell, B., Appold, M.S., Wilkinson, J.J., McClean, N.A. and Jeffries, T.E., 2008, Geochemistry and Evolution of Mississippi Valley-Type Mineralizing Brines from the Tri-State and Northern Arkansas Districts Determined by LA-ICP-MS Microanalysis of Fluid Inclusions. *Economic Geology* 103, 1411-1435.

- Suess, M.J., Mueller, E. & Wepf, R., 2011, Minimization of amorphous layer in Ar⁺ ion milling for UHR-EM. *Ultramicroscopy* 111(8), 1224-1232.
- Sverjensky, D.A., Shock, E.L. and Helgeson, H.C., 1997, Prediction of the thermodynamic properties of aqueous metal complexes to 1000 °C and 5 kb. *Geochimica et Cosmochimica Acta* 61, 1359-1421.
- Tagirov, B.R. and Seward, T.M., 2010, Hydrosulfide/sulfide complexes of zinc to 250°C and the thermodynamic properties of sphalerite. *Chemical Geology* 269, 301-311.
- Torpy, A., Wilson, N.C., MacRae, C.M., Pownceby, M.I., Biswas, P.K., Rahman, M.A. and Zaman, M.N., 2020, Deciphering the Complex Mineralogy of River Sand Deposits through Clustering and Quantification of Hyperspectral X-Ray Maps. *Microscopy and Microanalysis* 26, 768-792.
- Wilkinson, J.J., Stoffell, B., Wilkinson, C.C., Jeffries, T.E. and Appold, M.S., 2009, Anomalously Metal-Rich Fluids Form Hydrothermal Ore Deposits. *Science* 323, 764.
- Wilkinson, J., 2014, Sediment-Hosted Zinc-Lead Mineralization: Processes and Perspectives. *Treatise on Geochemistry: Second Edition Chapter 13*, Elsevier, 219-249.
- Wilkinson, J.J. and Hitzman, M.W., 2015, The Irish Zn-Pb Orefield: The View from 2014. *Current Perspectives on Zinc Deposits*. Irish Association for Economic Geology, pp. 59-72.
- Wolery, T.J., 1992, EQ3NR, A computer program for geochemical aqueous speciation-solubility calculations: Theoretical manual, user's guide, and related documentation (Version 7.0). Lawrence Livermore National Laboratory.